IEEE Access
Multidisciplinary | Rapid Review | Open Access Journal

Received August 9, 2019, accepted August 31, 2019, date of publication September 13, 2019,
date of current version September 30, 2019.

Digital Object Identifier 10.1109/ACCESS.2019.2941398

Use of Subarrays in Linear Array for Improving Wide Angular Scanning Performance

FANNUSH S. AKBAR[1], (Student Member, IEEE), L. P. LIGTHART[2], (Fellow, IEEE), GAMANTYO HENDRANTORO[1], (Senior Member, IEEE), AND I. E. LAGER[3], (Senior Member, IEEE)

[1]Department of Electrical Engineering, Institut Teknologi Sepuluh Nopember, Surabaya 60111, Indonesia
[2]IRCTR, Delft University of Technology, 2628 CD Delft, The Netherlands *(Retired)*
[3]Faculty of Electrical Engineering, Mathematics and Computer Science, Delft University of Technology, 2628 CD Delft, The Netherlands

Corresponding author: Fannush S. Akbar (fannush.akbar13@mhs.ee.its.ac.id)

This work was supported in part by the Indonesian Government through the Scholarship and Research Grant, under Grant 2014-2017 PMDSU.

ABSTRACT The scanning performance of wide-angular scanning linear arrays is primarily degraded by the limited angular profile of the employed elements' patterns. This paper introduces an innovative strategy for compensating this degradation by using subarrays. Our design uses a uniform linear array with half-wavelength spaced elements, supplemented by subarrays that are symmetrically placed at its edges. The employed subarrays have controlled patterns, favoring some directions for effective scan-loss compensation (SLC) and suppressing other directions for lowering the sidelobes level (SLL). Two types of feeding configurations, making use of fixed power dividers in combination with 1-bit phase switch, are used for producing the desired patterns. The complete array design and physical validation, starting from the elements, continuing with the subarrays and ending with the system integration are also discussed in detail. The integration of the subarrays yields notable performance improvements at large scanning angles when compared with uniform linear arrays. The peak and first SLL of −14.1 dB, and the SLC of 2 dB are obtained when the array with CUP antennas as elements is scanned to the maximum scan angle direction.

INDEX TERMS Phased array, scan-loss, sidelobe, subarray, wide-angular scanning.

I. INTRODUCTION

Modern radar applications are conditioned by the progress in the design and modular implementation of electronic beam scanning array antennas [1]. A particularly testing class of radar applications are those requiring circular beam scanning. Such a functionality is typically implemented via facetted architectures, in which case ensuring the facet-to-facet handover requires beam scanning within at least ±60° with respect to the facet's broadside. Concurrently, reliable target identification entails challenging upper bounds for sidelobe levels in terms of the first SLL (FSLL)– for sensitivity, and the peak SLL (PSLL)– for false-alarm mitigation.

Ensuring wide-angle scanning in phased arrays has long been known to be an exacting task, as demonstrated by early works such as [2]–[4]. More recently, studies have dealt primarily with the effects of mutual coupling [5]–[17] and scan-loss [18]–[23].

The associate editor coordinating the review of this manuscript and approving it for publication was Mohammad Tariqul Islam.

In this paper, we particularly focus on the scan-loss problem defined herein as the degradation of the array maximum gain with respect to that of the zero scan angle, which occurs due to the decaying pattern of the element at larger angles. Scan-loss compensation was achieved in [18]–[20] using a pattern-reconfigurable antenna (PRA) with an integrated adjustable element pattern to compensate the loss at large scan angles. A broad-beam antenna element was proposed for counteracting the element's beamwidth limitation [21]–[23]. At this point, we note that this superior performance was obtained at the expense of (occasionally, extreme) technological intricacies due to the complexity of the system and design.

Meanwhile, controlling the SLL in a linear array has also been investigated in the previous literature. The use of amplitude tapering for lowering the SLL was reported in [24], [25], but it leads to lower radiated power efficiency. In [26] and [27], the corporate series feeding was used for realizing the non-uniform amplitude. Another approach for mitigating the SLL by adopting non-uniform

element positions with uniform amplitudes was introduced in [28]–[30] and has been improved in [27] and [31]. However, the non-uniform placement of the array elements results in a low aperture efficiency. Lately, some researchers investigated such solutions as the combination of the amplitude tapering and non-uniform element positions [32], and the use of PRA [33]. However, such solutions lead to high system complexity and inflexibility.

Controlling SLL by using subarrays has been previously explored, examples being the sunflower concept [34], the overlapped arrays concept [35]–[37], or the approach in [38], [39]. Although these designs do deliver superior SLL performance, their practical implementation is intricate (specific tiles in [34] or complicated beam-forming networks [35], [36], [38], [39]). Moreover, they are only meant for broadside direction or extremely narrow beam scanning (a few degrees) [40].

Subarrays have also been used for wide-angular scanning applications, such as in [41] where a 2-element subarray consisting of broad-beam elements, with complicated design, is used. An innovative and effective approach for ensuring wide-angle scanning was proposed in [42] and [43]. For overcoming the scan-loss, those papers proposed accommodating *subarrays* with a purposefully tailored radiation pattern inside non-uniform arrays to provide scan-loss compensation (SLC). Specifically, *pattern-optimized subarrays* were inserted in the empty spaces inside a linear array generated via the deterministic placement in [30] and [44]. This strategy resulted into a 50 λ-long linear array (with λ being the free-space wavelength at the operating frequency f) providing lower than 3 dB peak directivity excursion and low FSLL over a $\pm 60°$ scanning range.

Building up on [42] and [43], the present paper discusses a highly innovative strategy for *simultaneously* compensating the scan-loss and lowering the SLL in linear arrays. This objective can be fulfilled by using subarrays with asymmetric patterns. Such patterns are obtained by adjusting the amplitude and phase of the subarray elements. Two types of subarrays, containing 2 and 3 elements, will be employed. These subarrays will be symmetrically placed at the array's edges for enabling beam scanning over a wide, symmetrical with respect to broadside, angular range. The array is fully implemented via Cavity-backed U-slotted Patched (CUP) antennas [43] that lend themselves to low-cost, single-layer printed-circuit-board (PCB) technology fabrication. The subarrays are designed in a modular manner, with the radiators and the feeding networks being realized on a common PCB board. For enabling the symmetric scanning, the feeding networks also incorporate a simple, 1-bit phase switch. Our design procedure also results in a linear array with uniform amplitude and fewer K-bit phase shifters than a dense array of the same length. All subarrays have been manufactured and fully validated via physical measurements. The full array performance was then inferred via off-line post-processing.

The paper is organized as follows: Section II discusses some conceptual prerequisites and the general array architecture. Section III concerns the design of the subarrays for lowering the scan-loss and SLL. The subarrays development via numerical simulations, fabrication and validation via physical measurements are presented in Section IV. In section V, the full array performance including optimum subarrays is evaluated. Finally, it is closed by formulating conclusions.

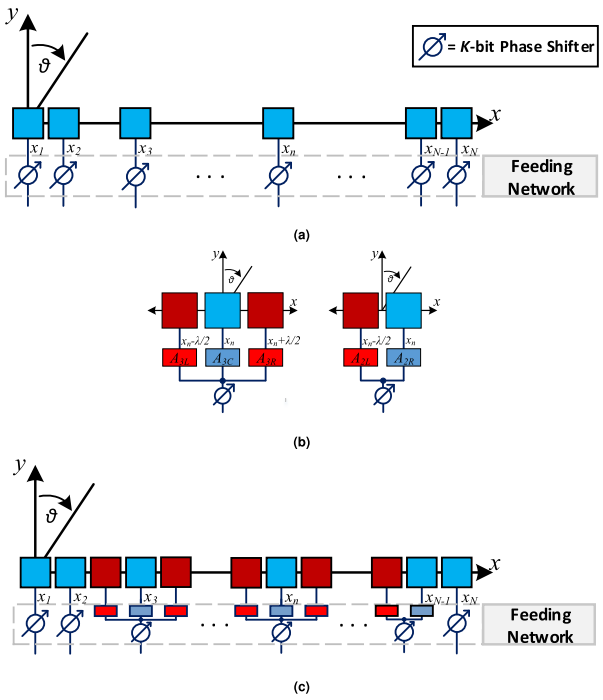

FIGURE 1. Examined configurations. (a) Linear array consisting of N radiators located along the x-axis; elements are fed via individual K-bit phase shifters. A K-bit phase shifter covers 2^K discrete phases; (b) Generic subarrays consisting of 3 elements and 2 elements; elements are $\lambda/2$-spaced, fed via a power divider attenuator; (c) The linear array from (a); elements at x_3, x_n, x_{N-1} being replaced by subarrays.

II. CONCEPTUAL BASIS

Consider an arbitrary linear, non-uniform array with N radiators located on a $\lambda/2$-spaced lattice along the x-axis, with elements located at x_n, with $n = 1, \ldots, N$ and $x_1 = 0$ (see Fig. 1a). The radiation pattern of the array is calculated for $\vartheta \in [-\pi/2, \pi/2]$, where ϑ measures the tilting with respect to the array broadside direction [45]. The progressive phase is employed in the standard manner for beam steering. The array is designed for wide angular scanning ($-60° \leqslant \vartheta \leqslant 60°$), scanning towards $\vartheta > 0°$ and towards $\vartheta < 0°$ being henceforth termed as "positive" and "negative" scanning directions, respectively.

As stated in the previous section, our strategy to SLC relies on integrating subarrays with an optimized pattern in the linear array configuration. There are two types of subarray configurations used in this paper, namely a 3-element and a 2-element one. Both configurations make use of phase-shifting networks, as shown in Fig. 1b. For each subarray, there is a reference element (printed in blue) located at, say,

x_n that also induces the subarray progressive phase shift at its input port. The other elements (in red) are spaced at $\lambda/2$. The subarray elements are each fed with a *fixed* amplitude and phase, these parameters being preset via power division networks. To be able to ensure the needed functionality, these power division networks also contain 1-bit, switch-based phase shifters.

The two types of subarrays have the following features:

- The 3-element subarrays are optimized (elements' amplitudes and phases) for lowering the SLL in conjunction with SLC. The amplitudes of the center, left and right side elements are defined as A_{3C}, A_{3L}, and A_{3R}, respectively, while the phases of the center, left and right side elements are defined as ψ_{3C}, ψ_{3L}, and ψ_{3R}, respectively (see left side figure of Fig. 1b).
- The 2-element subarrays are optimized (elements' amplitudes and phases) for enhancing the SLC. The amplitudes of the left and right side elements are defined as, A_{2L}, and A_{2R}, respectively, while ψ_{2L}, and ψ_{2R} are the phases of the left and right side elements, respectively (see right side figure of Fig. 1b).

For both subarrays, the phases of the left and right side elements have the same value but different signs for positive and negative scanning directions. Therefore, 1-bit phase switches are needed to switch the phase values of the left and right side elements for different scanning directions.

Subsequently, the optimized subarrays are integrated into the linear array. The new linear array including subarrays, located at x_3, x_n, x_{N-1} is shown in Fig. 1c. It is noticed that the number of phase controls in the transmit/receive (T/R) modules is determined by the sum of individual elements and subarrays. Moreover, there are two extra 1-bit phase switches per subarray for phase adjustment. The symmetrical placement of subarrays in the array is required in order to generate symmetric patterns for (near) broadside scanning while maintaining symmetric behavior for wide-angular, positive and negative scanning.

III. MODULAR SUBARRAY DESIGN

To design the subarray, target requirements should be determined, for example the scanning direction, the maximum scan angle, and the angular range in which the SLL needs to be lowered. A design with good SLC and low SLL while scanning over the angular domain in the area of $-60° < \vartheta < +60°$ is the main target. The amplitudes and phases of subarray elements are considered to achieve the target.

In [43], unequal symmetric subarray amplitudes and phases are used to produce an enhanced pattern at large angles. The enhanced subarray pattern could give the wanted SLC. However, this configuration leads to high SLL in other areas. Therefore, a novel analytical approach for designing subarrays to compensate for scan-loss while keeping SLL at an acceptable level is a major topic of the paper.

After a good subarray design has been obtained, the next step is realizing the modular subarray. For realization, a planar and PCB-based elementary radiator is proposed in order to achieve high-cost effectiveness. Besides that, microstrip-based power divider networks are also designed to produce the desired coupling values for feeding the subarray elements. All PCB-based designs in this paper are using Rogers with dielectric constant ϵ_r of 3.35 for the substrate material.

A. SUBARRAY DESIGN

Combining SLC with SLL suppression is optimally achieved by employing subarrays with a higher gain in (an angular interval around) the *array* scanning direction, and damped everywhere else. Since wide-angular scanning is aimed at, the subarrays are designed to favor the range $+30°$ to $+60°$ (positive scanning). To this end, we opt for scanning the *subarrays* at $+51°$, with an entailing progressive phase of $140°$ between subarray elements. These phase shifts must be reversed for scanning at negative directions. Note that, in order to level the SLL profile for broadside scanning (and, possibly, within a reduced angular range about broadside), symmetrically located subarrays will make use of a symmetric combination of subarray inter-element phase shifts. Since only one *fixed* phase shift is required within subarrays, this functionality can be straightforwardly implemented by using suitably chosen line lengths and switches, this amounting to implementing 1-bit, (true-time-delay) phase switch. Functionally, the needed combination of switched routes can be easily implemented in the array's control unit. To conclude with, the subarray elements are also placed on a $\lambda/2$ lattice. The two types of subarrays are now discussed separately.

1) 3-ELEMENT SUBARRAY

With reference to Fig. 1b, the elementary amplitudes are chosen as $A = [0.41; 0.82; 0.41]$, ensuring a unit-power at the subarray input feeding port and, moreover, a single-lobe radiation for broadside scanning (see [45, Section 6.8.3]). The subarray phase center coincides with that of the central element, that also gives the reference phase at the subarray feeding port. The phase shifts for the left and right elements, in this order, are chosen as $\pm 140°$ for positive scanning and $\mp 140°$ for negative scanning. The array factor (AF) of a 3-element subarray is shown in Fig. 2a. The pattern for positive scanning is maximized in the $35° < \vartheta < 60°$ range and minimized in the $-30° < \vartheta < -5°$ range, where SLL will be effectively suppressed, and the other way around for negative scanning.

2) 2-ELEMENT SUBARRAY

With reference to Fig. 1b, the elementary amplitudes are chosen as $A = [0.7; 0.7]$, corresponding to a uniformly-fed, 2-element array with unit-power at the subarray input feeding port. The subarray phase center is halfway between the two elements, implying for the selected $140°$ progressive phase (positive scanning) phase shifts of $\pm 70°$ for the left and right elements, respectively, with respect to the input port. The AF of the 2-element subarray is shown in Fig. 2b, the obtained pattern being largely similar to the one in Fig. 2a, with a maximized region in the $30° < \vartheta < 65°$ range and a

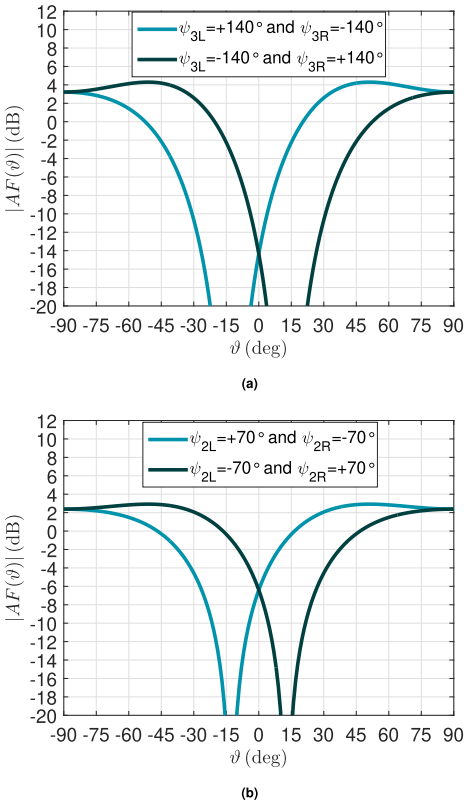

FIGURE 2. Optimized subarray factors with certain differential phase, ψ. (a) 3-element subarray with $\psi = \pm 140°$; (b) 2-element subarray with $\psi = \pm 70°$.

minimized one in the $-20° < \vartheta < -10°$ range for positive scanning.

B. ANTENNA ELEMENT DESIGN

The CUP antenna (see Fig. 3) is selected because it combines easy manufacturing with effective suppression of substrate coupling by means of the vias enclosing. The design and simulations have been discussed in [43]. Layout and dimensions of the CUP antenna design that operates at 3 GHz are also indicated there. The antenna is symmetric about the x-axis but asymmetric about the y-axis due to the shifted position of the feeding point.

C. POWER DIVIDER DESIGNS

The power dividers required by the subarray designs are designed and simulated in CST Microwaves Studio®. Two power divider designs are shown in the left-hand side of Fig. 4a and 4b, for the 2-way and 3-way power dividers, respectively. The 2-way power divider is designed based on a quadrature-hybrid coupler with port 1 as an input port, ports 2 and 3 as output ports with equal power, and port 4 as an isolated port terminated on a 50 Ω load. The desired phase difference between the output ports of 140° is implemented by extending the feeding lines.

The 3-way power divider design shown in Fig. 4b consists of two cascaded quadrature couplers with port 1 as an input port, and ports 2, 3 and 4 as output ports having powers

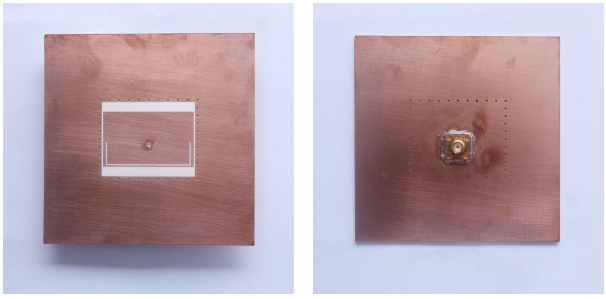

FIGURE 3. Fabricated CUP antenna, top (left side) and bottom (right side) view.

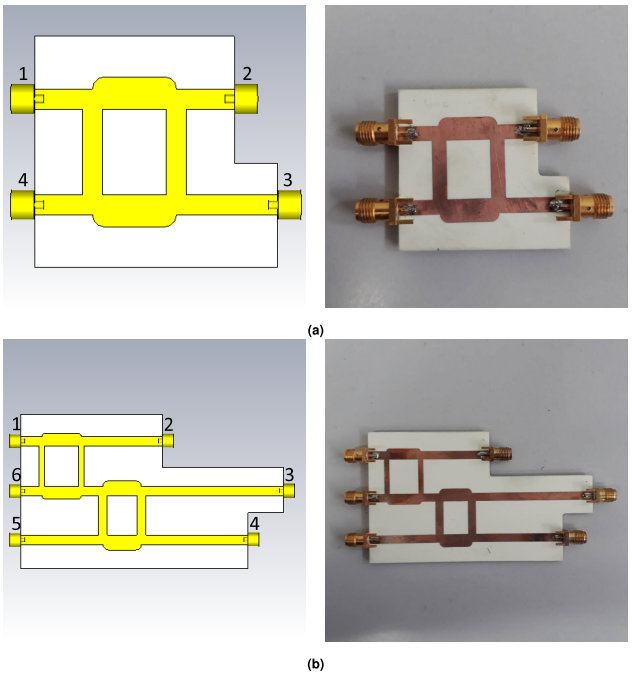

FIGURE 4. Power divider design (left-hand side figure) and fabrication (right-hand side figure) for validating the array performance for positive scan angles. (a) 2-way power divider; (b) 3-way power divider.

of 0.6724, 0.1681, and 0.1681, respectively. Note that port 2 feeds the center subarray element, while ports 3 and 4 feed the left and right sides elements, respectively. Those values correspond to the unit-power combination at the subarray input port of the element amplitudes $A = [0.41; 0.82; 0.41]$. Ports 5 and 6 are isolated ports and are terminated on 50 Ω loads.

IV. VALIDATION OF MODULAR SUBARRAYS

The modular subarrays described in the previous section have been manufactured. Measurement and simulation results are described in the following paragraphs.

A. PHYSICAL IMPLEMENTATION OF THE MODULAR SUBARRAYS

The CUP antenna was etched with double platted, drilling and via-platting. The SMA coaxial connector was

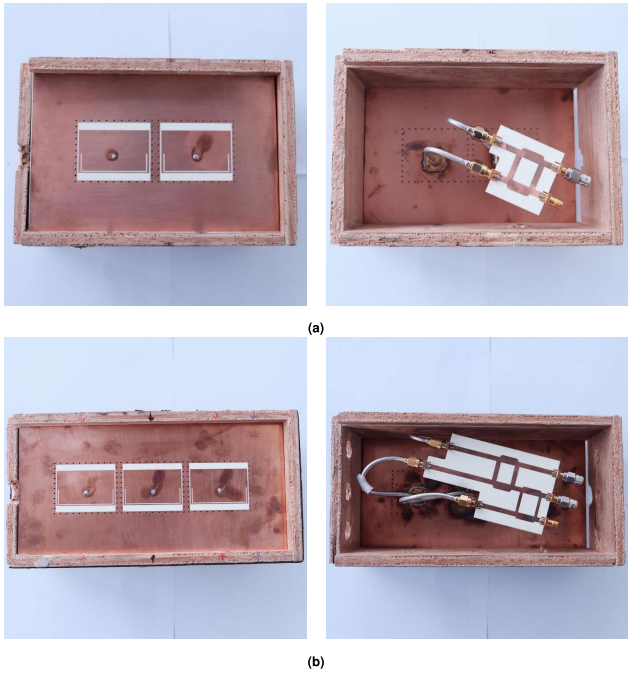

FIGURE 5. Fabricated modular subarrays, top (left) and bottom (right) view. (a) 2-element subarray; (b) 3-element subarray.

soldered manually. The manufactured antenna is displayed in Fig. 3 and the power dividers are shown in the right-hand side of Fig. 4a and 4b. Note that in the present implementation the phase shift is hardwired for positive scan angles. Clearly, the final realization will require a switchable line network for implementing the 1-bit phase switch. The fabricated 2-element and 3-element subarrays, including the power dividers, are displayed in Fig. 5a and 5b, respectively. The cables for different ports have different lengths for ensuring the correct phase shifts among the subarray elements.

B. MEASUREMENT SETUP

The manufactured subarrays, with the pertaining power dividers, were fully measured. Firstly, S-parameter measurements were carried out via a two-port VNA. All inactive ports were terminated with 50 Ω loads. The radiation patterns were measured in a small RF anechoic chamber. The antennas under test (AUT) were mounted on the non-metallic pole of the turntable, at 1 m height above the ground. Measurements were done via a standard-gain horn located at 2 m of the AUT, ensuring far-field conditions for the considered frequency and device dimensions. Pattern measurements are only reliable for angles between ±90° due to the existence of a power divider at the back of each subarray.

C. SIMULATED AND MEASURED SYSTEM PERFORMANCE OF THE MODULAR SUBARRAYS

The S_{11} simulation and measurement results of the CUP antenna are presented in Fig. 6a. It can be seen that the antenna is extremely well matched at 3 GHz, with a return loss of about −40 dB. The simulated and measured H-plane

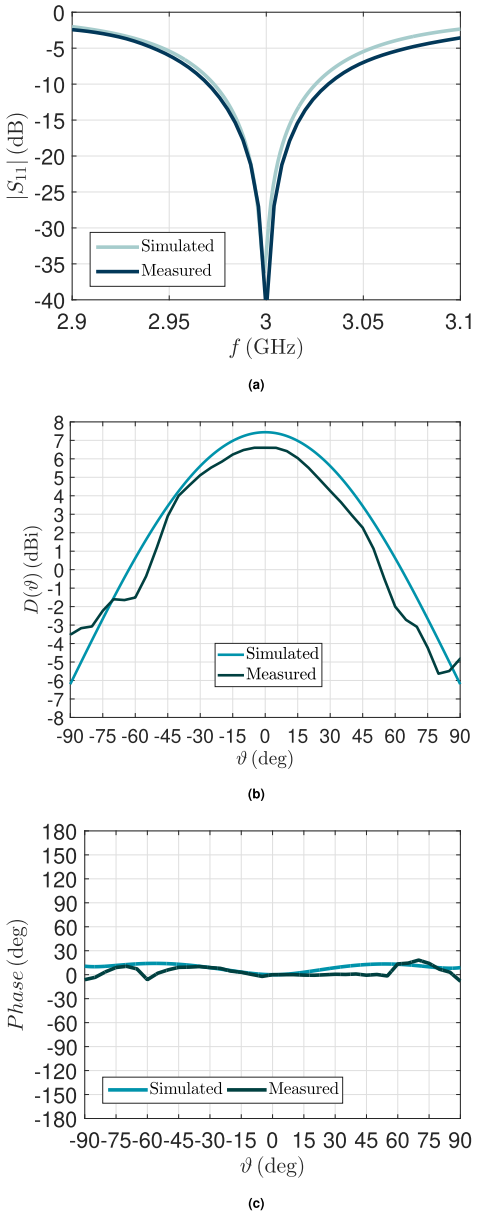

FIGURE 6. CUP antenna simulation [43] and measurement results. (a) $|S11|$; (b) H-plane magnitude pattern; (c) H-plane phase pattern.

patterns (see Fig. 6b) are also in good agreement, the small deviations being attributable to imperfections in the measurement setup, i.e. 0.8 dB difference between measured and simulated patterns at 0° direction. To conclude with, the phase pattern in Fig. 6c is almost flat.

The adequate performance of the 2-way and 3-way power dividers is illustrated in Fig. 7 - its discussion will focus on the measured results. To begin with, both power dividers show very good matching at the input port, with $|S_{11}|$ being below −15 dB over the examined bandwidth and below −25 dB at the operational frequency of 3 GHz. As for the insertion loss, in the case of the 2-way divider, the measured $|S_{21}|$ and $|S_{31}|$ reproduce remarkably well the required −3 dB transfer, with a negligible supplementary loss due to unavoidable

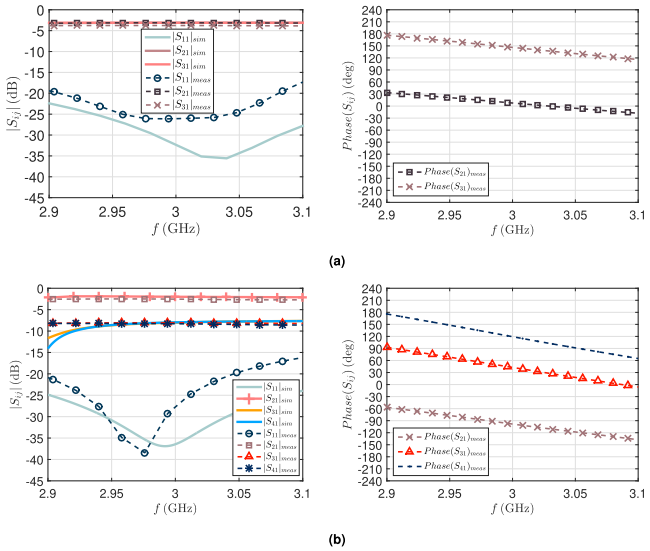

FIGURE 7. Simulation and measurement results of magnitude (left-hand side figure) and phase (right-hand side figure) S-parameters of power divider designs in Fig. 4. Note that correct phase values are obtained after adding a coaxial cable extension with a certain length in the measurement. (a) 2-way power divider; (b) 3-way power divider; the circularity of the phase is used for representing $Phase(S_{41})_{meas}$ for readability of the figure.

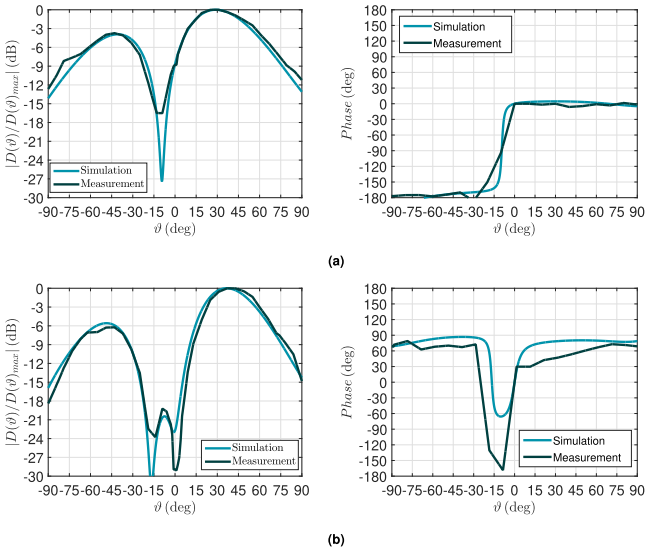

FIGURE 8. Simulation and measurement results of magnitude and phase patterns of modular subarrays with power divider in Fig. 4. (a) 2-element subarray; (b) 3-element subarray.

manufacturing inaccuracies. The same superior performance is observed in the case of the 3-way divider, in which case $|S_{21}|$, $|S_{31}|$ and $|S_{41}|$ are distinctively flat around the values of -2.4 dB, -8.1 dB, -8.2 dB, respectively, again in very good agreement with the design element amplitudes $A = [0.41; 0.82; 0.41]$ that were specified in III-A. For the phase measurements, additional calibrated lengths of semi-rigid coaxial cables were added at the output ports. In the case of the 2-way divider, a phase difference of 139° is obtained at the operational frequency, a very good replication of the required 140° phase shift. In the case of the 3-way divider, the phase difference between S_{21} and S_{41} is $217° = 360° - 143°$ and that between S_{21} and S_{31} is 141°, again in excellent agreement with the needed ±140° phase feeding. As expected, all phase plots are, practically, linear over the examined bandwidth. This implies that the patterns of the resulting subarrays and, later on, the full array are, for all purposes, independent from frequencies in that range.

Simulated and measured patterns of the modular subarrays at 3 GHz are presented in Fig. 8. The magnitude patterns of the 2-element subarray in the left-hand side of Fig. 8a have maxima around $\vartheta = +30°$ and minima around $\vartheta = -10°$, whereas the magnitude patterns of the 3-element subarray in the left-hand side of Fig. 8b exhibit maxima around $\vartheta = +35°$ and minima around $\vartheta = -15°$. These pattern characteristics are in agreement with the design. The phase patterns are presented on the right side of Fig. 8. Both the measured magnitude and phase patterns are in good agreement with the simulation results within ±90°. The measured subarray performance warrants their proper operation when integrated in the envisaged wide-angular-scanning linear arrays.

V. ARRAY ARCHITECTURE DESIGN

A. DESIGN STRATEGY

As elaborately discussed in the Introduction, precluding wide-angular scanning radiation degradation in combination with low SLL while also maintaining high radiation efficiency is a challenging task. Henceforth, a novel, effective strategy for achieving these operational goals is described:

1) Start with a $\lambda/2$-spaced, uniform linear array (ULA). Since the half-power beamwidth of the array is determined by the array length [46, Eq. (19.7.6)], the length of the array and, implicitly, the total number of elements N follows directly from the required beamwidth (a design specification).
2) Select a Taylor amplitude taper for ensuring the expected SLL; use this amplitude taper, via a moving average strategy, for thinning later in steps 3 and 4, with all kept elements being fed with the same (unit) amplitude.
3) Divide the ULA into a center part, and two symmetrical edge parts, depending on the corresponding moving average criterion: the center part corresponds to the region where the moving average is above a certain threshold – no thinning will be applied in that region; the remainder of the array will constitute the edge parts.
4) Carry out the thinning in the edge parts – this will yield empty spaces for accommodating subarrays.
5) Insert optimized subarrays in the empty spaces that can accommodate them – this will ensure SLC and a first-level SLL reduction.
6) Optimize the subarray positions to enhance SLL reduction.

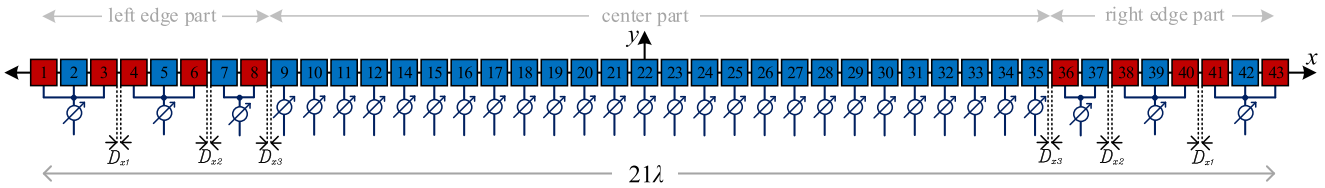

FIGURE 9. Final configuration of a linear array with integrated subarrays. Blue elements represent individually controlled elements (9, . . . , 35) or ON elements after thinning. Combinations of red/blue elements stand for subarrays. The subarrays are further spaced by additional spacings D_{x1}, D_{x2} and D_{x3} for enhanced SLC and SLL suppression. In the implementation, elements 3 and 4 are overlapped and so are 40 and 41, so that there are 41 elements left with 20λ length.

B. ARRAY ARCHITECTURE

The detailed description of the array synthesis starts from a linear λ/2-grid array with 41 elements, implying that the total array length is 20λ. The low SLL tapering used in the second step is a standard Taylor taper [45, Section 7.6] with −30 dB SLL. In step 3, we choose 0.64 as the threshold, being the average over all elements of the 5-point moving averaged Taylor-tapered amplitudes of the array. Applying this threshold, 21-element center part and two 10-element edges are obtained. However, later after thinning the edges in step 4, there are 3 edge elements, on each side, adjacent to the center part that are left ON and, consequently, are included into the center part. As the result, there are 27 elements in the center, i.e. elements 9 to 35 in Fig. 9, and 7 elements in each edge, i.e. elements 2 to 8 and 36 to 42.

To implement thinning on the edges, we apply ON/OFF condition to each element such that a 5-point moving average over all seven elements in one edge approximate the Taylor amplitudes in that area. The resulting thinned array is shown in Fig. 9 (blue elements). The ON elements are then replaced by subarrays with a unit amplitude, the resulting available space accommodating two 3-element and one 2-element subarrays. The edge-most elements, i.e. elements 2 and 42, each become the center element of a 3-element subarray by adding one extra element on each side. The total number of antenna elements now is 43, but the number of K-bit phase shifters is only 33 with extra 10 1-bit phase switches.

Step 6 in our design strategy amounts to optimizing the spacing between subarrays such that to enhance the SLL reduction. There are three distances that are optimized, namely D_{x1}, D_{x2}, and D_{x3}, indicated in Fig. 9. The optimization is conducted by using a grid search strategy. It is found that the optimum values are, $D_{x1} = -0.5\lambda$, $D_{x2} = 0.2\lambda$, and $D_{x3} = 0.1\lambda$. From the result, $D_{x1} = -0.5\lambda$ means that the neighbouring subarrays are overlapped: The right side element of the first 3-element subarray coincides with the left side element of the second 3-element subarray. When two elements coincide, the number of elements is reduced. In this case, there are 2 elements less, for both edge-parts. Therefore, the total number of elements becomes 41 with the same 33 + 10 phase controls. The feeding of the overlapped elements requires combining the signals that should have been fed to the corresponding elements in the initial 3-element subarrays. The relevant signals are combined via a phase-balanced power combiner and a delay line to correct the phase.

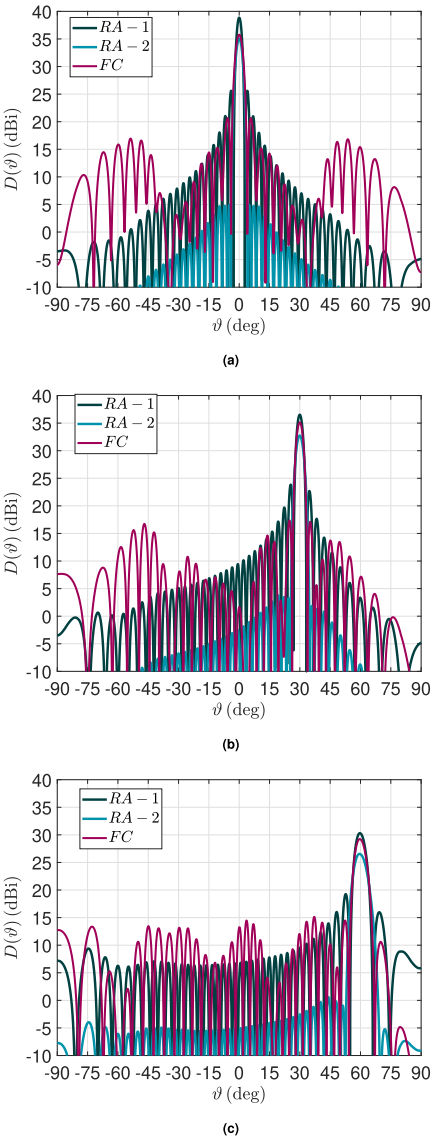

FIGURE 10. Comparison of the array patterns while scanning of 41-element ULA, 41-element with −30 dB Taylor and final configuration. (a) $\vartheta_0 = 0°$; (b) $\vartheta_0 = 30°$; (c) $\vartheta_0 = 60°$. For $\vartheta_0 = 0°$, the phases of subarray elements on both sides of the array are configured symmetrically around the array center.

TABLE 1. Summary of Radiation Patterns shown in Fig. 10.

Configuration Types	Number of Controls	Scanning ϑ_0	D_{max} (dBi)	Scan-loss (dB)	HPBW	FSLL (dB)	PSLL (dB)
41-element ULA (*RA-1*)	41 K-bit phase shifters	0°	38.8	0.0	2.4°	-13.2	-13.2
		30°	36.5	-2.3	2.8°	-12.7	-12.7
		60°	30.3	-8.5	4.9°	-11.1	-11.1
41-element -30 dB Taylor (*RA-2*)	41 K-bit phase shifters and 41 amplitude controls	0°	35.1	0.0	3.1°	-30.1	-30.1
		30°	32.7	-2.4	3.6°	-29.4	-28.9
		60°	26.6	-8.5	6.1°	-27.5	-25.9
Final Configuration (*FC*)	33 K-bit phase shifters and 10 1-bit phase switches	0°	35.8	0.0	3.5°	-15.1	-15.1
		30°	35.1	-0.7	3.1°	-17.8	-17.8
		60°	29.3	-6.5	5.5°	-14.7	-14.1

C. ARRAY VALIDATION

The pattern calculation is conducted in the post-processing by using the embedded element pattern method [47]. The element patterns (EP) are obtained from the measurement of CUP antennas arranged in a 3-element linear array configuration. The pattern comparison concerns the following arrays: (i) our final design, denoted as *FC*; (ii) a reference 41-element ULA, denoted as $RA-1$, having (approximately) the same length as our final design; (iii) a reference 41-element equally-spaced array with −30 dB Taylor taper, denoted as $RA-2$. The comparison for scan angles of 0°, 30° and 60° are shown in Fig. 10a, 10b, and 10c, respectively. The phases of the subarray elements are made to be symmetric to produce a symmetric pattern only for scanning in $-10° < \vartheta_0 < 10°$ and asymmetric for scanning to large angles. It can be seen that the mainlobe level of *FC* has less reduction while scanning to 60°, compared with the other two configurations. The best PSLL and FSLL are obtained from $RA-2$ due to the use of the amplitude tapering. The PSLL value is equal to FSLL for $RA-1$ and $RA-2$ due to their periodicity. Meanwhile, *FC* gives PSLL and FSLL values better than those of $RA-1$.

All key radiation performances while scanning shown in Fig. 10 are summarized in Table 1. The scan-loss of *FC* at 60° is only −6.5 dB instead of −8.5 dB which is the case in $RA-1$ and $RA-2$. The −8.5 dB scan-loss can be traced back to the EP magnitude at 60° of a measured CUP pattern. The half power beamwidth (HPBW) enlargement for *FC* while scanning is lower than the other two configurations, for which HPBW at $\vartheta_0 = 60°$ is twice the one corresponding to broadside scanning. Maximum FSLL and PSLL of *FC* for scanning to $\vartheta_0 = 60°$ are 0.4 dB and 1 dB lower than for $\vartheta_0 = 0°$, respectively. Meanwhile the FSLL and PSLL increment at larger scanning angle for the other configurations are more than 2 dB. Last but not least, the *FC* has 8 K-bit phase shifters less than the other two configurations and only add 10 1-bit phase switches.

To show the advantage of the proposed concept, the scan-loss as a function of (positive) scan angles is presented in Fig. 11. It can be seen that while scanning to 60° the maximum gains for $RA-1$ and $RA-2$ degrade by 8.5 dB, while the scan-loss of *FC* is increasing from broadside up to 20° and decreasing at larger scan angles. At 60° scan angle, it degrades by only 6.5 dB with respect to broadside scanning

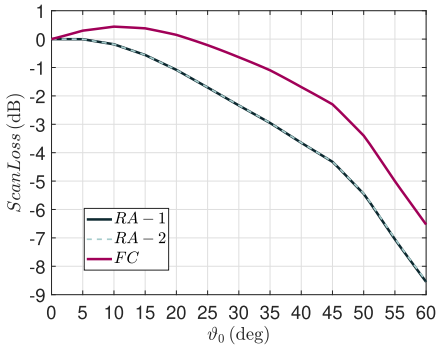

FIGURE 11. Scan-loss as function of (positive) scan angles comparison between 41-element ULA, 41-element with −30 dB Taylor and final configuration.

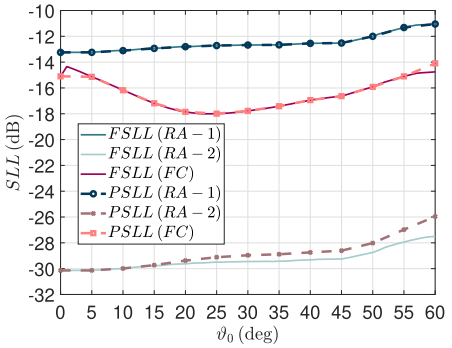

FIGURE 12. FSLL and PSLL as function of (positive) scan angles comparison between 41-element ULA, 41-element with −30 dB Taylor and final configuration.

direction. This demonstrates the compensation of the scan-loss. Moreover, the PSLL and FSLL as functions of (positive) scan angles shown in Fig. 12 also indicate the excellence of the proposed concept. The FSLL and PSLL with scan angle of *FC* are less increasing, while for the other two configurations, the increment is more remarkable. Although the SLL of $RA-2$ is always lower than *FC* and $RA-1$, $RA-2$ requires attenuators to realize the amplitude tapering, which also implies degradation in efficiency.

The above results demonstrate that the integration of subarrays into a linear uniform array following the previously outlined procedure is able to achieve wide angular scanning and a low SLL while maintaining the array efficiency.

VI. CONCLUSION

Design and experimental validation of the integration of modular subarrays in the linear array for lowering the scan-loss and SLLs at large scan angles due to the limited bandwidth of the EP have been reported. The design procedure has been presented, starting with a ULA with half-wavelength spacing being thinned at the edges to provide spaces for subarrays. The subarrays have controlled patterns, favoring some directions for an effective SLC and suppressing other directions to lower the SLL. To produce the desired patterns for positive and negative scan angles, two types of feeding configurations are used with fixed power dividers in combination with 1-bit phase switches.

The experimental validation using an array with CUP elements and employing two 3-element subarrays and one 2-element subarray at each edge shows that it outperforms a ULA with half-wavelength spacings of the same length in scan-loss, SLL and the number of phase controls. When the dense array is Taylor-tapered for −30 dB SLL, the array with integrated subarrays is only worse in SLL, but excels in scan-loss, power efficiency and the number of controls. A strong and prime conclusion for using subarrays can, therefore, be that the integrated optimized subarrays are giving substantial performance improvement for a linear array antenna.

REFERENCES

[1] E. Brookner, "Phased-array and radar astounding breakthroughs—An update," in *Proc. Radar Conf.*, May 2008, pp. 1–6.
[2] G. Farrell, Jr., and D. Kuhn, "Mutual coupling in infinite planar arrays of rectangular waveguide horns," *IEEE Trans. Antennas Propag.*, vol. AP-16, no. 4, pp. 405–414, Jul. 1968.
[3] G. , H. Knittel, A. Hessel, A. , and A. Oliner, "Element pattern nulls in phased arrays and their relation to guided waves," *Proc. IEEE*, vol. 56, no. 11, pp. 1822–1836, Nov. 1968.
[4] E. Magill and H. Wheeler, "Wide-angle impedance matching of a planar array antenna by a dielectric sheet," *IEEE Trans. Antennas Propag.*, vol. 14, no. 1, pp. 49–53, Jan. 1966.
[5] D. M. Pozar, "The active element pattern," *IEEE Trans. Antennas Propag.*, vol. 42, no. 8, pp. 1176–1178, Sep. 1994.
[6] H. Vo, *Development of an Ultra-Wideband Low-Profile Wide Scan Angle Phased Array Antenna*, The Ohio State Univ., Columbus, OH, USA, 2015. [Online]. Available: https://etd.ohiolink.edu
[7] C.-C. Chen, "Broad-band impedance matching of rectangular waveguide phased arrays," *IEEE Trans. Antennas Propag.*, vol. AP-21, no. 3, pp. 298–302, May 1973.
[8] J. A. Kasemodel, C.-C. Chen, and J. L. Volakis, "Wideband planar array with integrated feed and matching network for wide-angle scanning," *IEEE Trans. Antennas Propag.*, vol. 61, no. 9, pp. 4528–4537, Sep. 2013.
[9] G. Oliveri, F. Viani, N. Anselmi, and A. Massa, "Synthesis of multilayer WAIM coatings for planar-phased arrays within the system-by-design framework," *IEEE Trans. Antennas Propag.*, vol. 63, no. 6, pp. 2482–2496, Jun. 2015.
[10] M. Li, S.-Q. Xiao, and B.-Z. Wang, "Investigation of using high impedance surfaces for wide-angle scanning arrays," *IEEE Trans. Antennas Propag.*, vol. 63, no. 7, pp. 2895–2901, Jul. 2015.
[11] R. Wang, B.-Z. Wang, X. Ding, and X.-S. Yang, "Planar phased array with wide-angle scanning performance based on image theory," *IEEE Trans. Antennas Propag.*, vol. 63, no. 9, pp. 3908–3917, Sep. 2015.
[12] W. H. Syed, D. Cavallo, H. T. Shivamurthy, and A. Neto, "Wideband, wide-scan planar array of connected slots loaded with artificial dielectric superstrates," *IEEE Trans. Antennas Propag.*, vol. 64, no. 2, pp. 543–553, Feb. 2016.
[13] G. Yang, J. Li, R. Xu, Y. Ma, and Y. Qi, "Improving the performance of wide-angle scanning array antenna with a high-impedance periodic structure," *IEEE Antennas Wireless Propag. Lett.*, vol. 15, pp. 1819–1822, 2016.
[14] E. Yetisir, N. Ghalichechian, and J. L. Volakis, "Ultrawideband array with 70° scanning using FSS superstrate," *IEEE Trans. Antennas Propag.*, vol. 64, no. 10, pp. 4256–4265, Oct. 2016.
[15] L. Gu, Y.-W. Zhao, Q.-M. Cai, Z.-P. Zhang, B.-H. Xu, and Z.-P. Nie, "Scanning enhanced low-profile broadband phased array with radiator-sharing approach and defected ground structures," *IEEE Trans. Antennas Propag.*, vol. 65, no. 11, pp. 5846–5854, Nov. 2017.
[16] D. Cavallo, W. H. Syed, and A. Neto, "Connected-slot array with artificial dielectrics: A 6 to 15 GHz dual-pol wide-scan prototype," *IEEE Trans. Antennas Propag.*, vol. 66, no. 6, pp. 3201–3206, Mar. 2018.
[17] Y. Liu, H. Yang, Z. Jin, and J. Zhu, "An improvement approach for wide-angle impedance matching using ELC metasurface slabs for SIW slot array antennas," *Int. J. Antennas. Propag.*, vol. 2018, Apr. 2018, Art. no. 3164147.
[18] Y.-Y. Bai, S. Xiao, M.-C. Tang, Z.-F. Ding, and B.-Z. Wang, "Wide-angle scanning phased array with pattern reconfigurable elements," *IEEE Trans. Antennas Propag.*, vol. 59, no. 11, pp. 4071–4076, Nov. 2011.
[19] S. Xiao, C. Zheng, M. Li, J. Xiong, and B.-Z. Wang, "Varactor-loaded pattern reconfigurable array for wide-angle scanning with low gain fluctuation," *IEEE Trans. Antennas Propag.*, vol. 63, no. 5, pp. 2364–2369, May. 2015.
[20] Z. Jiang, S. Xiao, and Y. Li, "A wide-angle time-domain electronically scanned array based on energy-pattern- reconfigurable elements," *IEEE Antennas Wireless Propag. Lett.*, vol. 17, no. 9, pp. 1598–1602, Sep. 2018.
[21] Y.-F. Cheng, X. Ding, W. Shao, and C. Liao, "A high-gain sparse phased array with wide-angle scanning performance and low sidelobe levels," *IEEE Access*, vol. 7, pp. 31151–31158, 2019.
[22] G. Yang, J. Li, D. Wei, and R. Xu, "Study on wide-angle scanning linear phased array antenna," *IEEE Trans. Antennas Propag.*, vol. 66, no. 1, pp. 450–455, Jan. 2018.
[23] G. Yang, J. Li, S. G. Zhou, and Y. Qi, "A wide-angle E-plane scanning linear array antenna with wide beam elements," *IEEE Antennas Wireless Propag. Lett.*, vol. 16, pp. 2923–2926, 2017.
[24] T. T. Taylor, "Design of line-source antennas for narrow beamwidth and low side lobes," *Trans. IRE Prof. Group Antennas Propag.*, vol. 3, no. 1, pp. 16–28, Jan. 1955.
[25] A. Villeneuve, "Taylor patterns for discrete arrays," *IEEE Trans. Antennas Propag.*, vol. AP-31, no. 10, pp. 1089–1093, Oct. 1984.
[26] S. Ogurtsov and S. Koziel, "On alternative approaches to design of corporate feeds for low-sidelobe microstrip linear arrays," *IEEE Trans. Antennas Propag.*, vol. 66, no. 7, pp. 3781–3786, Jul. 2018.
[27] H. Khalili, K. Mohammadpour-Aghdam, S. Alamdar, and M. Mohammad-Taheri, "Low-cost series-fed microstrip antenna arrays with extremely low sidelobe levels," *IEEE Trans. Antennas Propag.*, vol. 66, no. 9, pp. 4606–4612, Sep. 2018.
[28] R. Harrington, "Sidelobe reduction by nonuniform element spacing," *IRE Trans. Antennas Propag.*, vol. 9, no. 2, pp. 187–192, Mar. 1961.
[29] R. Willey, "Space tapaering of linear and planar arrays," *IRE Trans. Antennas Propag.*, vol. 10, no. 4, pp. 369–377, Jul. 1962.
[30] D. G. Leeper, "Isophoric arrays-massively thinned phased arrays with well-controlled sidelobes," *IEEE Trans. Antennas Propag.*, vol. 47, no. 3, pp. 1825–1835, Dec. 1999.
[31] G. Buttazzoni and R. Vecovo, "Reducing the sidelobe power pattern of linear broadside arrays by refining the element positions," *IEEE Antennas Wireless Propag. Lett.*, vol. 17, no. 8, pp. 1464–1468, Aug. 2018.
[32] X. Ma, Y. Liu, K. Da Xu, C. Zhu, and Q. H. Liu, "Synthesising multiple-pattern sparse linear array with accurate sidelobe control by the extended reweighted L1-norm minimisation," *Electron. Lett.*, vol. 54, no. 9, pp. 548–550, May 2018.
[33] J.-C. Wu, C.-C. Chang, T.-Y. Chin, S.-Y. Huang, and S.-F. Chang, "Sidelobe level reduction in wide-angle scanning array system using pattern-reconfigurable antennas," in *IEEE MTT-S Int. Microw. Symp. Dig.*, May 2010, pp. 1274–1277.
[34] M. C. Viganó, G. Toso, G. Caille, C. Mangenot, and I. E. Lager, "Sunflower array antenna with adjustable density taper," *Int. J. Antennas Propag.*, vol. 2009, Jan. 2009, Art. no. 624035.
[35] D. Petrolati, P. Angeletti, and G. Toso, "A lossless beam-forming network for linear arrays based on overlapped sub-arrays," *IEEE Trans. Antennas Propag.*, vol. 62, no. 4, pp. 1769–1778, Apr. 2014.
[36] S. P. Skobelev, "Some features of the overlapped subarrays built up of beam-forming matrices for shaping flat-topped radiation patterns," *IEEE Trans. Antennas Propag.*, vol. 63, no. 12, pp. 5529–5535, Dec. 2015.

[37] D. Bianchi, S. Genovesi, and A. Monorchio, "Randomly Overlapped Subarrays for Angular-Limited Scan Arrays," *Prog. Electromagn. Res. C*, vol. 68, pp. 129–139, 2016. doi: 10.2528/PIERC16060602.
[38] G. Oliveri, M. Salucci, and A. Massa, "Synthesis of modular contiguously clustered linear arrays through a sparseness-regularized solver," *IEEE Trans. Antennas Propag.*, vol. 64, no. 10, pp. 4277–4287, Oct. 2016.
[39] P. Rocca, M. A. Hannan, L. Poli, N. Anselmi, and A. Massa, "Optimal phase-matching strategy for beam scanning of sub-arrayed phased arrays," *IEEE Trans. Antennas Propag.*, vol. 67, no. 2, pp. 951–959, Feb. 2019.
[40] R. Haupt, "Reducing grating lobes due to subarray amplitude tapering," *IEEE Trans. Antennas Propag.*, vol. AP-33, no. 8, pp. 846–850, Aug. 1985.
[41] Y.-F. Cheng, X. Ding, W. Shao, and B.-Z. Wang, "Dual-band wide-angle scanning phased array composed of SIW-cavity backed elements," *IEEE Trans. Antennas Propag.*, vol. 66, no. 5, pp. 2678–2683, May. 2018.
[42] F. S. Akbar, L. P. Ligthart, I. E. Lager, and G. Hendrantoro, "Subarrays in linear array configurations, an effective instrument for scan loss compensation," in *Proc. LAPC*, Nov. 2016, pp. 1–5.
[43] F. S. Akbar, L. P. Ligthart, G. Hendrantoro, and I. E. Lager, "Scan loss mitigation via subarrays a full-scale concept demonstrator," in *Proc. EuMC*, Oct. 2017, pp. 156–159.
[44] M. Skolnik, G. Nemhauser, and J. Sherman, "Dynamic programming applied to unequally spaced arrays," *IRE Trans. Antennas Propag.*, vol. 12, pp. 1825–1835, Jan. 1964.
[45] C. A. Balanis, *Antenna Theory: Analysis and Design*, 4th ed. New York, NY, USA: Wiley, 2016.
[46] S. J. Orfanidis. *Electromagnetic Waves and Antennas*. Accessed: Jul. 4, 2019. [Online]. Available: https://www.ece.rutgers.edu/~orfanidi/ewa
[47] D. Kelley, "Embedded element patterns and mutual impedance matrices in the terminated phased array environment," in *Proc. IEEE Antennas Propag. Soc. Int. Symp.*, Jul. 2005, pp. 659–662.

FANNUSH S. AKBAR (S'15) received the B.A.Sc. degree in telecommunication engineering from Politeknik Elektronika Negeri Surabaya (PENS), Surabaya, Indonesia, in 2013. He is currently pursuing the Ph.D. degree in electrical engineering with the Institut Teknologi Sepuluh Nopember (ITS), Surabaya. His recent research interests include phased array antenna with wide-angular scanning capability, array synthesis, and microstrip antennas.

L. P. LIGTHART was born in The Netherlands, in September 1946. He received the degree in engineering *(cum laude)* and the Ph.D. degree from the Delft University of Technology.

Since 1988, he has been the Chair on MW transmission, remote sensing, radar, and positioning and navigation with the Delft University of Technology. He founded the IRCTR at Delft University, where he is currently an Emeritus Professor, and the Guest Professor with Universities in Indonesia and China, and the Chairman of CONASENSE. He gives various courses on radar, remote sensing in antennas and published more than 650 articles, various book chapters, and books. He has supervised more than 50 Ph.D. students. His research interests include antennas and propagation, radar and remote sensing, satellite, and mobile and radio communications. He is a member BoG of the IEEE-AESS and a Fellow of IET and the Academician of the Russian Academy of Transport. He is also a Founding Member of the EuMA, the Chaired 1st EuMW, in 1998, and an Initiated EuRAD, in 2004. He received Honorary Doctorates at MSTUCA, Moscow, Tomsk State University and MTA Romania.

GAMANTYO HENDRANTORO was born in Jombang, Indonesia, in November 1970. He received the B.Eng. degree in electrical engineering from the Institut Teknologi Sepuluh Nopember (ITS), Surabaya, Indonesia, in 1992, and the M.Eng. and Ph.D. degrees in electrical engineering from Carleton University, Ottawa, ON, Canada, in 1997 and 2001, respectively.

He is currently a Professor with the Department of Electrical Engineering, ITS. His current research interests include radio propagation channel modeling and wireless communications. He has been involved in various studies, including investigation into millimeter-wave propagation, channel modeling and wireless systems for tropical areas, studies on HF skywave channels and communications in equatorial regions, and the development of radar array and signal processing.

I. E. LAGER (SM'14) received the M.Sc. degree in electrical engineering from the Transilvania University of Braşov, Romania, in 1987, the Ph.D. degree in electrical engineering from the Delft University of Technology, Delft, The Netherlands, in 1996, and the Ph.D. degree in electrical engineering from the Transilvania University of Braşov, in 1998. He successively occupied several research and academic positions with the Transilvania University of Braşov and the Delft University of Technology, where he is currently an Associate Professor. In 1997, he was a Visiting Scientist with Schlumberger-Doll Research, Ridgefield, CT, USA. He also investigates effective methods for teaching electromagnetic field theory at (under) graduate level. His research interests include applied electromagnetics, especially time-domain propagation and applications, and antenna engineering, with an emphasis on nonperiodic (interleaved) array antenna architectures.